
Research Article: Confirmation | Disorders of the Nervous System

Deficit in motor skill consolidation-dependent synaptic plasticity at motor cortex to Dorso Lateral Striatum synapses in a mouse model of Huntington's disease

<https://doi.org/10.1523/ENEURO.0297-19.2020>

Cite as: eNeuro 2020; 10.1523/ENEURO.0297-19.2020

Received: 31 July 2019

Revised: 23 January 2020

Accepted: 29 January 2020

This Early Release article has been peer-reviewed and accepted, but has not been through the composition and copyediting processes. The final version may differ slightly in style or formatting and will contain links to any extended data.

Alerts: Sign up at www.eneuro.org/alerts to receive customized email alerts when the fully formatted version of this article is published.

Copyright © 2020 Glangetas et al.

This is an open-access article distributed under the terms of the Creative Commons Attribution 4.0 International license, which permits unrestricted use, distribution and reproduction in any medium provided that the original work is properly attributed.

1 **Title:** Deficit in motor skill consolidation-dependent synaptic plasticity at motor cortex to
2 Dorso Lateral Striatum synapses in a mouse model of Huntington's disease

3 **Abbreviated title:** Motor skills consolidation in Huntington's disease mouse model

4 **List of Authors:** Christelle Glangetas*, Pedro Espinosa* and Camilla Bellone#

5 Department of Basic Neuroscience, University of Geneva, 1, rue Michel-Servet, Geneva,
6 Switzerland

7 Author contribution

8 * Authors contributed equally to this work

9 # Corresponding author email: camilla.bellone@unige.ch

10

11 **Author contributions:**

12 *Ex vivo* electrophysiology experiments and behavioural tasks were performed by C.G and
13 P.E.. P.E. and C.G. analyzed the *in vitro* electrophysiology data and the behavioural
14 experiments. P.E. and C.G. performed the statistical analyses for the *in*
15 *vitro* electrophysiology and the behavioral experiments. The study was designed and the
16 manuscript written by C.B., C.G., with assistance from P.E.

17 **Correspondence should be address to:** camilla.bellone@unige.ch

18 Pages 28

19 Figures 6

20 Abstract 165 words

21 Significance statement 115 words

22 Introduction 711 words

23 Discussion 1460 words

24

25 **Conflicts of Interest:**

26 The authors have no conflicts of interest.

27 **Acknowledgments**

28 C.B. is supported by the Swiss National Science Foundation and by Synapsis foundation.

29 P.E. is also supported by the Swiss Government Excellence Scholarship (FCS) for PhD
30 studies ESKAS-Nr: 2017.0922. We thank Lorena Jourdain for the technical assistance, all
31 the members of the Bellone's laboratory for critical discussions. We thank Manuel Mameli,
32 Vincent Pascoli, Francis Chaouloff for critical reading of the manuscript.

33

34 **Funding sources:**C.B. is supported by the Swiss National Science Foundation and by
35 Synapsis foundation. P.E. is also supported by the Swiss Government Excellence Scholarship
36 (FCS) for PhD studies ESKAS-Nr: 2017.0922.

37

38 **Deficit in motor skill consolidation-dependent synaptic plasticity at motor cortex to**
39 **Dorso Lateral Striatum synapses in a mouse model of Huntington's disease**

40

41 Abbreviated title: Motor skills consolidation in Huntington's disease mouse model

42

43 Christelle Glangetas*, Pedro Espinosa* and Camilla Bellone#

44 Department of Basic Neuroscience, University of Geneva, 1, rue Michel-Servet, Geneva,
45 Switzerland

46

47 * Authors contributed equally to this work

48 # Corresponding author email: camilla.bellone@unige.ch

49

50 Pages 28

51 Figures 6

52 Abstract 165 words

53 Significance statement 115 words

54 Introduction 711 words

55 Discussion 1460 words

56

57 **Conflicts of Interest:**

58 The authors have no conflicts of interest.

59

60 **Acknowledgments**

61 C.B. is supported by the Swiss National Science Foundation and by Synapsis foundation.

62 P.E. is also supported by the Swiss Government Excellence Scholarship (FCS) for PhD

63 studies ESKAS-Nr: 2017.0922. We thank Lorena Jourdain for the technical assistance, all

64 the members of the Bellone's laboratory for critical discussions. We thank Manuel Mameli,

65 Vincent Pascoli, Francis Chaouloff for critical reading of the manuscript.

66

67

68

69 **Abstract**

70 Huntington's disease (HD) is a neurodegenerative disease notably characterized by
71 progressive motor symptoms. Although the loss of Medium Spiny Neurons (MSNs) in the
72 striatum has been associated with motor deficits, premanifest patients already present
73 cognitive deficiencies and show early signs of motor disabilities. Here in a YAC128 HD
74 mouse model, we identified impairment in motor skill consolidation at the age of 11 - 14
75 weeks. Using optogenetic stimulation, we found that excitatory synaptic transmission from
76 motor cortex to MSNs located in the Dorso Lateral part of the Striatum (DLS) is altered.
77 Using single pellet reaching task, we observed that while motor skill consolidation is
78 accompanied by a dynamic change in AMPA/NMDA ratio in wild type mice, this form of
79 synaptic plasticity does not occur in YAC128 mice. This study not only proposes new
80 meaningful insight in the synaptopathic mechanisms of HD, but also highlights that deficit in
81 motor skill consolidation-dependent synaptic plasticity at motor cortex to DLS synapses
82 represents an early biomarker for Huntington's disease.

83
84

85 **Significance Statement**

86
87 Huntington's disease (HD) is a neurodegenerative disease characterized by prominent motor
88 manifestations in addition to nonmotor changes in behavior and cognition. Several studies
89 have provided evidences that the neuropathological hallmark of HD begins and progresses
90 before the conventional diagnosis can be made. Here using an animal model, we identified
91 deficit in motor skill in early stage of the disease. Remarkably these early behavioural deficits
92 are accompanied by aberrant plasticity at synapses between motor cortex and dorsal striatum.
93 This study not only gives a better understanding in the synaptopathic mechanisms of HD, but
94 also highlights that deficit in motor skill consolidation-dependent synaptic plasticity at motor
95 cortex to dorsal striatum synapses represents an early biomarker for Huntington's disease.

96
97

98 **Introduction**

99

100 Huntington's disease (HD) is an autosomal dominant neurodegenerative disease caused by
101 CAG repetition in the gene encoding huntingtin protein (HTT) and is characterized by
102 progressive motor, cognitive and psychiatric symptoms. Neurodegeneration of Medium
103 Spiny Neurons (MSNs) in the striatum is the principal pathological hallmark of HD (la
104 Monte et al., 1988). Although MSNs degeneration has been associated with motor deficits,
105 premanifest patients already present cognitive deficiencies (Giralt et al., 2012) and show
106 subtle signs of motor disabilities (Tabrizi et al., 2011). Indeed, slight impairment in motor
107 coordination, in fine motor control of upper extremities and in motor sequence learning have
108 been described in premanifest HD patients (de Boo et al., 1997) (Kirkwood et al., 1999)
109 (Kirkwood et al., 2000) (Tabrizi et al., 2009) (Schneider et al., 2010). It has been therefore
110 proposed that fine motor evaluation may represent an early biomarker of the disease (Duff et
111 al., 2008).

112

113 Several mechanisms attempted to explain how mutated HTT (mHTT) protein leads to
114 neuronal dysfunction without cell death in premanifest HD. Reduced striatal activity and
115 changes in synaptic properties in the striatum have been described both in human and in
116 mouse models (Wolf et al., 2012; Milnerwood and Raymond, 2010). In particular, increased
117 sensitivity to NMDA (Levine et al., 1999) and increased extrasynaptic NMDAR signaling
118 (Milnerwood et al., 2010) have been observed at early stage of the disease. These data
119 suggest that dysfunctions in NMDA transmission may occur early in the disease progression.
120 NMDARs are heteromeric receptors containing GluN1 subunits together with a combination
121 of GluN2 (A-D) and/or GluN3 (A, B) subunits. Subunit composition determines the
122 receptor's biophysical and pharmacological properties and changes in NMDAR subunit
123 composition contribute to the pathophysiology of several neurological diseases (Paoletti et
124 al., 2013). The expression of both GluN2B and GluN3A subunits have been previously
125 linked to HD. Extrasynaptic GluN2B-containing NMDARs are enriched in the striatum of
126 transgenic mice expressing mutated full-length human HD gene (YAC128) at an age
127 preceding motor dysfunctions (Milnerwood et al., 2010). Elevated GluN3A expression has
128 been observed in both HD mouse models and human patients and linked to abnormal
129 excitation of MSNs in the striatum (Marco et al., 2013; Mahfooz et al., 2016). Although early
130 postsynaptic changes in NMDAR-mediated transmission have been described in premanifest
131 HD mouse models, it is still an open question whether these changes only impact

132 survival/death signaling balance and consequent neuronal degeneration or whether they could
133 also be causally link to early behavioural phenotypes.

134

135 New motor skill learning is often characterized by a fast-initial phase of improvement of the
136 performance followed by a gradual progress of motor skills. After consolidation, memory
137 becomes long-lasting and can persist for the entire life. Several studies have indicated that the
138 striatal circuits and the synaptic mechanisms engaged during early and late phase of skill
139 learning differ. Specifically, while changes in Dorso Medial Striatum (DMS) have been
140 predominantly observed during early training, changes in Dorso Lateral Striatum (DLS) have
141 been only detected after extensive training (Yin et al., 2009). Subjects with premanifest HD
142 exhibit learning impairment with no differences in initial performance prior to the time of
143 clinical diagnosis (Shabbott et al., 2013). The neuronal mechanisms underlying these deficits
144 are still largely unknown. Interestingly in mice it has been previously shown that
145 consolidation of motor skills is accompanied by long-lasting changes in glutamatergic
146 transmission onto MSNs and requires striatal NMDAR (Dang et al., 2006; Yin et al., 2009;
147 Lambot et al., 2016). Whether deficits of synaptic plasticity in HD could underlying motor
148 skill deficits represents an interesting hypothesis.

149

150 Here, using YAC128 HD mouse model, we found that between the age of 11 - 14 weeks,
151 mice show impairment in motor skill consolidation. Using optogenetic stimulation, we have
152 observed a decrease in AMPA/NMDA ratio at motor cortex to DLS MSN synapses. This
153 change was accompanied by a change in NMDA receptor subunit composition and by an
154 aberrant NMDA-dependent form of long-term depression at motor cortex to DLS when
155 compared to control mice. Remarkably, using single pellet reaching task, we found that
156 motor skill consolidation was accompanied by a reduction in AMPA/NMDA ratio in wild
157 type mice. This form of synaptic plasticity was absent in YAC128 mice suggesting that the
158 decreased AMPA/NMDA ratio in YAC128 mice limits consolidation of motor skills in
159 premanifest HD.

160

161

162 **Materials and Methods**

163

164 **Animals**

165 YAC128 homozygote in a FVB/N background (line 55) crossed into a C57Bl6J background
166 (4 back-crosses) were obtained from Perez Otano laboratory (as previously described in
167 (Marco et al 2018). YAC128 homozygous were intercrossed with Tg(Drd1-dtTomato)
168 heterozygous transgenic mice (generous gift from Pr. N. Deglon; C57BL6/j background) to
169 generate YAC128 heterozygous-Drd1-dtTomato heterozygous mice. We then crossed
170 YAC128 heterozygous-Drd1-dtTomato heterozygous mice to generate YAC128
171 homozygous-Drd1-dtTomato mice (YAC128-D1) selected with real-time quantitative PCR
172 analysis. We then used YAC128 homozygous-Drd1-dtTomato mice from YAC128
173 homozygous-Drd1-dtTomato mice crossing with YAC128 homozygous or YAC128
174 homozygous-Drd1-dtTomato mice. Both YAC128 homozygous and YAC128 homozygous
175 Drd1-dtTomato positive mice were used for *in vitro* electrophysiology and behaviors as
176 similar phenotypes were observed regardless of Drd1-dtTomato genotype (data not shown).
177 In parallel, we crossed Tg(Drd1-dtTomato) heterozygous transgenic mice with WT YAC128
178 mice (selected from YAC128 heterozygous crossing) to generate WT Drd1-dtTomato mice.
179 Both age and genetic background matched WT Drd1-dtTomato transgenic mice without
180 differentiate homozygosity from heterozygosity for Drd1-dtTomato (which can be a
181 limitation point in this study) and C57BL6/j were used as controls in this study. WT and
182 YAC128 mice are not generated from same breeding pairs and parental behaviors were not
183 taken into considerations in this study. Both males and females were respectively housed in
184 groups with food and water *ad libitum* under controlled conditions (22-23°C, humidity 50 ± 5
185 %, 12 h light-dark cycle with light on at 7.00 a.m). All the procedures performed at the
186 UNIL and UNIGE compiled with the Swiss National Institutional Guidelines on Animal
187 experimentation and were approved by the Swiss Cantonal Veterinary Office Committee for
188 Animal Experimentation. VD 3016.d license authorization.

189

190 **Electrophysiology**

191 250 µm thick coronal slices containing dorsolateral striatum were prepared following the
192 experimental injection protocols described in the text. Slices were kept in artificial
193 cerebrospinal fluid containing 119 mM NaCl, 2.5 mM KCl, 1.3 mM MgCl₂, 2.5 mM CaCl₂,
194 1.0 mM NaH₂PO₄, 26.2 mM NaHCO₃ and 11 mM glucose, bubbled with 95% O₂ and 5%
195 CO₂. Slices were maintained 30 min in bath at 30°C and then at room temperature. Whole-

196 cell voltage-clamp recording techniques were used (37°C, 2–3 ml min⁻¹, submerged slices)
197 to measure the holding currents and synaptic responses of dorsolateral striatum MSN. The
198 internal solution contained 130 mM CsCl, 4 mM NaCl, 2 mM MgCl₂, 1.1 mM EGTA, 5 mM
199 HEPES, 2 mM Na₂ATP, 5 mM sodium creatine phosphate, 0.6 mM Na₃GTP and 0.1 mM
200 spermine. Currents were amplified, filtered at 5 kHz and digitized at 20 kHz.

201 Access resistance was monitored by a hyperpolarizing step of -4 mV at each sweep, every 10
202 s. The cells were recorded at the access resistance from 10–25 MΩ for MSN. Data were
203 excluded when the resistance changed > 25%. Synaptic currents were evoked by intrastriatal
204 electrical stimulation at 0.1 Hz and 0.05–0.1 msec of duration. For optogenetic experiments,
205 we stimulated the glutamatergic fibers from motor cortex or from the thalamus in the
206 dorsolateral striatum. The stimulus was delivered at 0.1 Hz and the duration was 1-3 msec.
207 The experiments were carried out in the presence of GABA_A receptor antagonist picrotoxin
208 (100 μM); the AMPAR-EPSCs were pharmacologically isolated by application of the
209 NMDAR antagonist D-APV (50 μM) and NMDAR EPSCs were recorded at +40 mV in
210 presence of the AMPAR blocker NBQX (10 μM). Representative example traces are shown
211 as the average of 15-20 consecutive EPSCs typically obtained at each potential. The
212 rectification index of AMPARs is the ratio of the chord conductance calculated at negative
213 potential (-60 mV) divided by the chord conductance at positive potential (+40 mV). The
214 analysis of the decay time of NMDAR-mediated EPSC was conducted as described
215 previously and the Ifenprodil sensitivity was calculated as the percentage of NMDAR-EPSC
216 amplitude reduction (at + 40 mV) after 20-25 minutes of continuous Ifenprodil (3 μM,
217 GluN2B-containing NMDAR antagonist) bath-application compared to baseline. The time
218 interval between the two stimulations for the Paired Pulse Ratio (PPR) measurement was 50,
219 100 and 300 msec (Inter Stimulation Interval, ISI) and the ratio was obtained by dividing the
220 EPSC2 by EPSC1 amplitude at - 60 mV.

221 For the in vitro validation of the optogenetic experiment and the strontium chloride
222 experiment, the internal solution contained 140 mM K-Gluconate, 2 mM MgCl₂, 5 mM KCl,
223 0.2 mM EGTA, 10 mM HEPES, 4 mM Na₂ATP, 0.3 mM Na₃GTP and 10 mM Creatine-
224 Phosphate. Blue-light was delivered through the 40X objective focused on the cell soma. The
225 Synaptic responses were collected with a Multiclamp 700B-amplifier (Axon Instruments,
226 Foster City, CA), filtered at 2.2 kHz, digitized at 10 Hz, and analyzed online using Igor Pro 6
227 software (Wavemetrics, Lake Oswego, OR).

228 I-V curves of pharmacologically isolated NMDARs were generated holding the cells at
229 different membrane potential for 5 min each and normalizing EPSCs at 40 mV.

230 Asynchronous evoked EPSC (aEPSC). For this experiment, 3 mM of SrCl₂ was added in the
231 aCSF solution instead of the CaCl₂. The internal solution contained: 140 mM K-Gluconate, 2
232 mM MgCl₂, 5 mM KCl, 0.2 mM EGTA, 10 mM HEPES, 4 mM Na₂ATP, 0.3 mM Na₃GTP
233 and 10 mM Creatine-Phosphate. Cells were held at – 70mV, and picrotoxin was added in this
234 external bath. Asynchronous events were measured during 180 ms period, between 20 ms to
235 200 ms after stimulation (Choi and Lovinger 1997). Quantal events were detected and
236 analysed using Mini analysis program version 6.0.

237 The plasticity experiments were recorded at -40 mV holding potential, we measured 10
238 minutes of baseline response at 0.1 Hz, followed by 5 minutes of stimulation at 1 Hz. Then
239 we recorded the EPSCs for 40 minutes.

240

241 **Stereotaxic injections**

242 AAV5-CamKII-hChR2(H134R)-EGFP virus has been injected in the Motor Cortex in 4 to 7
243 weeks old mice. Anesthesia was induced and maintained with a mixture of Oxygen and
244 Isoflurane. The animals were then placed on the stereotaxic frame (Stoelting Co., USA) and a
245 single or bilateral craniotomy was made over Motor Cortex at following stereotaxic
246 coordinates: M1: AP +1.18 mm, ML 1.21 mm, DV 0.65 mm from Bregma; M2: AP +1.18
247 mm, ML 0.60 mm, DV 0.50 mm from Bregma and for the thalamus at following coordinates:
248 AP -2.30 mm, ML 0.6 mm, DV 3 mm from Bregma. The virus was injected with graduated
249 pipettes (Drummond Scientific Company, Broomall, PA) at the rate of 100 nL/min for a total
250 volume of 200 nL per injection side. For all the experiments the virus was incubated for at
251 least 4 weeks, when expression was clearly identifiable by the reporter protein expression,
252 before proceeding with further manipulations.

253

254 **Circular corridor test**

255 Mice were placed in a circular corridor (30 cm diameter) and were allowed to freely explore
256 the circular corridor for a 30 min period in 11 lux illumination condition. Total distance
257 travelled and velocity during the session were automatically recorded (Ethovision, Noldus,
258 Wageningen, the Netherlands). Arena was cleaned with 1% acetic acid and dried between
259 each test.

260

261 **Open field test**

262 Mice were placed in a square open field (42×42 cm) and were allowed to freely explore the
263 open field for a 10 min period in 11 lux illumination condition. Total distance travelled and

264 velocity during the session were automatically reported (Ethovision, Noldus, Wageningen,
265 the Netherlands). The arena was cleaned with 1% acetic acid and dried between each test.

266

267 **Single pellet reaching task test**

268 To evaluate motor skill learning, a single pellet reaching task was performed. This paradigm
269 requires a precise and coordinated sequence of movements of the forelimb in a serial order.

270 Mice are trained to extend their forelimbs through a narrow slit to grasp and retrieve millet
271 pellets (food) positioned at a fixed location as described in Chen et al 2014. First, mice are
272 placed on a food restriction schedule, 90 % of their free feeding body weight (Chen et al
273 2014, Lambot et al 2016). In detail, food restriction starts two days prior experiment to
274 initiate bodyweight loss. In a second step, group and individual habituation have been done in
275 the training chamber. In details, two cagemate mice are placed in the training chamber
276 (custom made transparent Plexiglas training chamber 20 cm tall, 15 cm deep, 8.5 cm wide
277 that contains three vertical slits) at the same time with 20 millet pellets inside the chamber for
278 20 min. The next day, a single habituation as previously described has been accessed (see the
279 figure 2A-B). Then, to determine the forelimb dominance, a food platform with millet pellets
280 was placed in front of the training chamber to allow the accessibility of the pellets to the
281 mouse through vertical slit of the training chamber. This shaping phase is achieved when two
282 criteria were encountered 1) the mouse conducts 20 reaching attempts within 20 min and 2)
283 more than 70% reaching attempts are performed with one forelimb. If the mouse does no
284 attempt these criteria within one week, the mouse was then excluded from the experiment.
285 After this shaping phase (5 days), a single-pellet training started (8 days). During the training
286 phase, mice are trained to reach single pellet for 20 min per day. After training, mice returned
287 to their home cage and were kept under food restriction. Three responses were manually
288 scored: success (grasp the pellet with the preferred paw and put it in the mouth), drop (grasp
289 the pellet with the preferred paw and release it before to put in the mouth) and fail (can't
290 grasp the pellet with the preferred paw). Speed of success is defined as the number of
291 successful reaches per minute. Success rate is the number of successful reaches divided by
292 total reaching attempts (success/(success+ drop+ fail attempts)) expressed in percentage. Fail
293 rate is the number of fail reaches divided by total reaching attempts (fail/(success+ drop+ fail
294 attempts)) expressed in percentage. During the entire experiment, mice are group-housed (age
295 and sex matches). All the procedure was recorded with a camera JVC model No. GZ-
296 R430BE. 1 YAC128 and 1 WT mice have been excluded according to the exclusion criteria.

297

298 **Rotarod test**

299 Mice were brought 30 min prior the experiment in the room to allow acclimatization. The
300 rotarod apparatus (Ugo Basile, Biological Research Apparatus, Varese, Italy) consisted of a
301 plastic roller with small grooves running along its turning axis. Mice received 2 trials per day
302 for 4 consecutive days, then the training was interrupted for 2 days, after this period the
303 training restarted for 2 additional days. The protocol consists in a classical accelerated
304 rotarod (Southwell et al., 2009) from 5 rotations per minute (RPM) to 40 RPM within 240 sec
305 ramping over a maximum duration of 300s with 10 min interval session break. We scored the
306 mouse fall latency in seconds of each last trial session per day. Mice that did not fall during
307 experiment were scored as 300s.

308

309 **Swimming tank test**

310 To measure swimming behavior, we used a swimming tank apparatus build of Plexiglas, the
311 dimensions were 100 cm long, 30 cm high and 6 cm wide with an escape platform in one
312 extremity (6x6 cm and 20 cm high) (Carter et al., 1999). The tank was filled with water (26-
313 27°C) until the escape platform protrudes 1-2 cm above the water level. In the opposite side
314 of the platform, a vertical red line indicates the starting point located at 60 cm from the
315 platform. The first day of training, the animals were deposited in the tank and when necessary
316 were conducted to reach the platform. From day 2 of training, animals were deposited and
317 slightly conducted until the red line. The task consists in three consecutive trials
318 (approximately 10 seconds between trails), performed daily from Day 1 to 3. After 3 days of
319 recovery, we run the last training session (day 7). We measured the time to swim the 60 cm
320 of distance from the red line to the platform. Trials were finished when mice reached and
321 climbed on the platform. Given that YAC128 mice expressed a floating behavior during this
322 task we set a threshold time of 30 seconds, if mice completed the task in more than 30 s, the
323 trials were counted as failed. In the figure **1H** we used *Drd1* td tomato mice as WT and
324 *Drd1*td tomato-YAC128 as YAC128. We have also performed the same experiments in
325 C57BL6/J and YAC128 and there was no difference in the performance with insertion of *D1*
326 td tomato allele (data not shown).

327

328 **Elevated plus maze**

329 The elevated plus maze consisted in a platform of four opposite arms (40 cm) two of them are
330 open and two are closed arms (enclosed by 15 cm high walls). The apparatus was elevated at
331 55 cm from the floor. The task was recorded and analyzed with the software Ethovision

332 (Noldus, Wageningen, the Netherlands) and we measured the time spent in each arm in trials
333 of 5 min. The luminosity of the room was 11-12 Lux in the open arms.

334

335 **Sucrose preference test**

336 Mice were housed individually after the end of the single pellet reaching task for the duration
337 of this task (3 days) and had access to standard lab chow and tap water throughout the
338 experiment. At 6.00 p.m., they were exposed to two drinking bottles, one containing water
339 and the other one with a sucrose solution. During the first two days, sucrose was given at 1%
340 and the third day, the sucrose solution was given at 8% concentration. Every day, the sucrose
341 and the water consumption were weighted. Water and sucrose bottle positions were
342 counterbalanced to avoid any confounding effect of side preference. Sucrose and water
343 consumption were measured for each mouse and a sucrose preference ratio was calculated
344 (sucrose consumed/ (sucrose consumed + water consumed)). 1 WT mouse has been excluded
345 for the Day 1 of sucrose consumption due to a problem in the sucrose bottle.

346

347 **Real-Time PCR**

348 Real time PCR was performed by microsynth company to determine the genotype of the
349 transgenic YAC128 mice. Genomic DNA was isolated from ear punch or postmortem tail
350 biopsies and analyzed by real -time PCR specific for huntingtin gene and β -actin. The
351 resulting Ct values are used for relative quantification of the copy-number of human specific
352 huntingtin (HD) in the provided samples according to the following equation: $\Delta Ct = Ct(\beta$
353 $actin) - Ct(HD)$. The gene expression fold change, normalized to the β -actin and relative to
354 the control sample, was calculated as $2^{-\Delta Ct}$. Values close to 1 corresponds to HD
355 homozygous while values lower than 0.5 corresponds to HD heterozygous mice. All samples
356 were run in triplicate. The following primers used for the real-time PCR reaction were:

357 HD primer:

358 F 5' GAAAGTCAGTCCGGGTAGAACTTC 3'

359 R 5' CAGATACCCGCTCCATAGCAA 3'

360 mouse b-actin primers:

361 F 5' ACGGCCAGGTCATCACTATTG 3'

362 R 5' CAAGAAGGAAGGCTGGAAAAGA 3'

363 Briefly, real time PCR was assayed in a total volume of 20 μ L reaction mixture containing
364 2.5 μ L of diluted cDNA, 10 μ L SYBR Green PCR master mix (Applied Biosystem), 1 μ L
365 primer F (5pmol/ μ L), 1 μ L primer R (5pmol/ μ L), 5.5 μ L H₂O. PCR thermal conditions were

366 done with a step at 50 °C for 2 min, a 10 min at 95 °C, followed by 40 cycles of denaturation
367 for 15 s at 95 °C and annealing/primer elongation for 1 min at 60 °C.

368

369 **Drug and viruses**

370 AAV5-CamKII-hChR2(H134R)-EYFP virus (2.8×10^{12} viral molecules/mL, UNC GTC
371 Vector core), D-AP5 (0106, Tocris), Picrotoxin (1128, Tocris), NBQX (0373, Tocris),
372 Ifenprodil hemitartrate (0545, Tocris).

373

374 **Statistical Analysis**

375 Normality was checked with the Shapiro-Wilk criterion and when violated, non-parametric
376 statistics were applied (Mann-Whitney and Kruskal-Wallis). When samples were normally
377 distributed, data were analyzed with independent or paired two-tailed samples t-tests, one-
378 way, two-way or repeated measures analysis of variance (ANOVA) followed if significant by
379 post hoc tests. All error bars represent the mean \pm the standard error of the mean (SEM) and
380 the significance was set at $p < 0.05$. Data were analyzed using the Graphpad Prism 5 and 7
381 and graphs were created using the Graphpad Prism 5 and 7 (San Diego, CA, USA). Outliers
382 were defined as higher than mean ± 2 SD (standard deviation). In all the electrophysiological
383 experiments we excluded 10 cells in total, 6 WT and 4 YAC128.

384

385

386 **RESULTS**

387 YAC128 mice show strong motor dysfunctions when they reached 10 months (Marco et al.,
388 2013) while earlier detection of motor disturbance in this model is more controversial (Slow
389 et al., 2003; Southwell et al., 2009; Van Raamsdonk et al., 2005; 2007; Pouladi et al., 2009).
390 To verify whether subtle deficits in motor behavior could be observed at earlier time points,
391 we tested mice between 11 and 14 weeks. We did not detect any gross impairment in
392 locomotor activity as indicated by the absence of differences in travelled distance and
393 velocity between Wild Type (WT) and YAC128 mice in the circular corridor (distance
394 travelled: WT: 39.98 ± 3.64 m, N= 6 mice; YAC128: 41.91 ± 3.91 m, N=6 mice, $t(10)=0.3603$
395 unpaired t-test $p > 0.05$; velocity WT: 0.02 ± 0.002 m/s; YAC128: 0.02 ± 0.002 m/s,
396 $t(10)=0.3419$ unpaired t-test $p > 0.05$ **Fig. 1A-C**) and in the open field tests (distance travelled:
397 WT: 3.24 ± 0.37 m; YAC128: 3.27 ± 0.31 m, $t(10)=0.06773$ unpaired t-test $p > 0.05$; velocity
398 WT: 0.07 ± 0.01 m/s; YAC128: 0.07 ± 0.02 m/s, U=15 Mann Whitney test $p > 0.05$ **Fig. 1D-**
399 **F**). However, in the swimming tank test (**Fig. 1G**) while independently on the genotype, mice
400 present equivalent initial behavior at day 1 and improve the time to cross the tank at day 2,
401 only WT mice maintain their performance over the following days (Friedman test for WT,
402 $F(4)=11.40$ $p=0.004$; N= 6 mice, Friedman test for YAC128 mice, $F(4)=18.21$ $p=0.0004$, N=
403 9 mice, Mann-Whitney test for WT D1 vs YAC128 D1 $p=0.9305$, Mann-Whitney test for
404 WT D7 vs YAC128 D7 $p=0.0004$ **Fig. 1H**). During the test, in YAC128 mice we also
405 observed an increased number of failed trials (**Fig. 1I**) compared to controls and the
406 appearance of floating behavior (**Fig. 1J-K**). Although we cannot exclude that YAC128 mice
407 took more time to reach the platform across days compared to WT as consequence of the
408 emergence of floating behavior, our data suggest that early stages of the disease are
409 characterized by deficits in consolidation of the motor performance in the swimming tank
410 test.

411 We performed an elevated plus maze to evaluate whether YAC128 mice present an anxiety
412 phenotype at this early stage. We observed that YAC128 mice spent less time in the open
413 arms compared to WT (WT 3.650 ± 0.6 %, N= 16 mice, YAC128 1.686 ± 0.3 %, N= 19
414 mice , $p < 0.005$; Mann-Whitney test, **Fig. 1L-M**) suggesting an anxiety-like phenotype in
415 these mice at early stage of the disease.

416 To assess motor learning abilities of YAC128 mice, we used the accelerated rotarod task
417 (**Fig. 1N**). Rotarod task allow us to observe the acquisition and the consolidation of a new
418 motor skill (Karni et al 1998). While no differences in the time to fall were observed at day 1
419 and 4 (**Fig. 1O**), YAC128 mice did not improved their performance over the days and

420 differences between mice were observed at day 7 and day 8 (Two way Anova main effect of
421 genotype $F(1.96)=13.85$, $p<0.001$ followed by Bonferroni post hoc, WT D7 255.6 ± 13.15 s,
422 $N=20$ mice, YAC128 D7 191.9 ± 14.72 s, $N=14$ mice, $p<0.005$, **Fig.10**).

423

424 To study fine motor skill learning involving forelimb dexterity, we then adopted the single-
425 pellet reaching task. In this task, food restricted mice were trained to extend their forelimbs
426 through a narrow slit to grasp and to retrieve food pellets positioned in a fixed location. After
427 2 days of habituation, mice underwent 5 days of shaping followed by a period of training
428 (**Fig. 2A-B**; See Material and method session). YAC128 and control mice showed similar
429 performance at the first training session. Strikingly, while control mice still improved the
430 successful attempts per minute after a break (Day 8), YAC128 mice did not enhance their
431 performance (**Fig. 2C-D**) (Two way Anova interaction effect $F(2.48)=4.32$, $p<0.05$, followed
432 by a Bonferroni post hoc WT D8 4.578 ± 0.5809 successful attempts per minute $N=9$ mice,
433 YAC128 D8 2.133 ± 0.4052 successful attempts per minute, $N=9$ mice $p<0.01$, **Fig. 2D**). In
434 addition, successful rate increased between day 1 versus day 8 in WT while it remained
435 unchanged in YAC128 mice (Paired t-test for WT D1: 37.56 ± 7.120 , D8: 53.89 ± 2.6 ,
436 $t(8)=2.397$ $p<0.05$ and for YAC128 D1: 39.44 ± 4.1 D8: 43.0 ± 3.0 , $t(8)=0.7702$ $p>0.4633$
437 **Fig 2E-F**). Alteration in single pellet reaching task in YAC128 mice does not account for
438 difference in bodyweight compared to WT across the task (data not shown), neither for
439 differences in total attempts or fail rate across days between groups (Fails: Two way Anova
440 interaction effect $F(6.112)=0.714$, $p>0.05$, no main effect; Drop: Two way Anova interaction
441 effect $F(6.112)=1.071$, $p>0.05$, and no main effect **Fig. 2G-H**), nor for general anhedonia
442 (lack of interest in a rewarding stimulus) as indicated by no difference in sucrose preference
443 test (sucrose preference , WT D2: 0.67 ± 0.06 ; YAC128 D2: 0.66 ± 0.03 ; Mann Whitney
444 $p>0.05$; WT D3: 0.82 ± 0.05 ; YAC128 D3: 0.85 ± 0.01 , Mann Whitney $p>0.05$, **Fig 2 I-M**).
445 These data suggest that at early stages of the disease, HD mice present difficulties in the
446 consolidation of newly acquired motor skills.

447

448 Changes in excitatory synaptic transmission in the striatum have been previously described in
449 symptomatic HD mouse models. Here we first investigated whether early behavioral traits
450 were accompanied by specific changes in glutamatergic synaptic transmission onto MSN in
451 the DLS. Using intra-striatal electrical stimulation (**Fig. 3A**), we did not detect changes in
452 presynaptic release properties (WT 1.01 ± 0.04 , $n=14$ neurons; YAC128 1.01 ± 0.03 , $n=10$
453 neurons, Unpaired t test, $t(22)=0$, $p>0.05$, 1 outlier WT) **Fig. 3B**), neither in the amplitude

454 and frequency of strontium-evoked asynchronous AMPAR events (WT $20 \pm 0,81$ pA , n= 6
455 neurons; YAC128 $20,62 \pm 1,29$ pA, n= 10 neurons, Mann Whitney test $U =27$ $p>0.05$; WT
456 13.39 ± 3 Hz; YAC128 15.69 ± 2.21 Hz Unpaired t-test $t(14)=0.6266$ $p>0.05$ **Fig 3C**).
457 Furthermore, we did not detect change in the strength of synaptic transmission measured as
458 AMPA/NMDA ratio (WT $0,56 \pm 0,03$ n=9 neurons; YAC128 $0,50 \pm 0,06$, n= 9 neurons
459 Unpaired t-test $t(15)=1.054$ $p>0.05$ **Fig. 3D**). When we pharmacologically isolated AMPARs
460 we did not detect any change in rectification index (WT $0,93 \pm 0,07$ n=14 neurons; YAC128
461 $1,05 \pm 0,07$, n=10 neurons, Unpaired t-test $t(24)=1.165$ $p>0.05$ **Fig. 3E**), suggesting that
462 YAC128 mice at this age do not present GluA2-lacking AMPARs. When we
463 pharmacologically isolated NMDARs, ifenprodil sensitivity was not different between
464 YAC128 and control mice (WT $33,09 \pm 4,13$ %, n=8 neurons; YAC128 $43,13 \pm 8,18$ % n=8
465 neurons , Unpaired t-test $t(16)=0.9795$ $p>0.05$ **Fig. 3 F-G**), suggesting that NMDA subunit
466 composition was not changed in YAC128 mice compared to control.

467
468 DLS receives major glutamatergic inputs from motor cortex and thalamus. These inputs have
469 different functional properties and early deficits within specific circuits may lead to deficits
470 in motor skill learning. Using optogenetic tools, we here investigated whether we could
471 detect changes in glutamatergic transmission from motor cortex and thalamus onto DLS
472 MSNs (Smith et al., 2004) (Wall et al., 2013; Guo et al., 2015). First, we injected
473 Channelrodhopsin (ChR2) expressing virus in the motor cortex and in the thalamus in control
474 and YAC128 mice (**Fig. 4A**). After 6 weeks, acute brain slices were obtained and recording
475 were performed from MSN of the DLS. We did not detect differences in the strength of
476 transmission at thalamo-DLS synapses (WT $0,57 \pm 0,11$; n=11 neurons; YAC128 $0,48 \pm$
477 $0,11$; n=7 neurons Unpaired t-test $t(16)=0.4942$ $p>0.05$ **Fig. 4B**). By contrast, when we
478 recorded light-evoked synaptic transmission from motor cortex inputs to DLS MSNs, we
479 found a decreased AMPA/NMDA ratio in YAC128 compared to WT (WT $0,57 \pm 0,04$ n=22
480 neurons; YAC128 $0,41 \pm 0,05$ n=19 neurons Mann Whitney $U=124$ $p<0.05$ **Fig. 4C**)
481 affecting both $D1^+$ MSN and $D1^-$ MSNs (WT $D1^+$ 0.642 ± 0.06 , n=8 neurons, WT $D1^-$ 0.554
482 ± 0.08 , n=7 neurons, YAC128- $D1^+$ 0.426 ± 0.08 , n= 9 neurons , YAC128- $D1^-$ $0.355 \pm$
483 0.05 , n= 9 neurons, Two way Anova interaction effect $F(1.31)=0.4294$, $p>0.05$, Genotype
484 main effect $F(1.31)=8.518$, $p=0.006$, **Fig. 4D**). The rectification index of AMPAR-mediated
485 transmission (WT $0,95 \pm 0,1$ n=8 neurons; YAC128 $0,83 \pm 0,06$ n=13 neurons Man Whitney
486 test $U=38$ $p>0.05$ **Fig. 4E**), amplitude of the optically-induced AMPAR mediated currents
487 (WT, n=8 neurons; YAC128, n=13 neurons **Fig. 4F**) as well as the amplitude of strontium-

488 evoked asynchronous AMPAR events (WT $18,86 \pm 0,57$ pA n=16 neurons; YAC128 $18,66 \pm$
489 $1,07$ pA n=7 neurons Unpaired t-test $t(21)=0.1854$ $p>0.05$ **Fig. 4G**) did not differ between
490 control and YAC128 mice. Furthermore, we did not observe changes in the paired pulse ratio
491 measured at different time intervals (WT 50 ms : $0,41 \pm 0,06$ n=15 neurons; YAC128 50 ms:
492 $0,38 \pm 0,05$ n=11 neurons Unpaired t test $t=0.3778$ $p>0.05$, WT 100 ms: $0,74 \pm 0,06$;
493 YAC128 100 ms: $0,56 \pm 0,08$ Unpaired t test $t=1.938$, $p=0.064$, WT 300 ms: $0,76 \pm 0,08$;
494 YAC128 300 ms: $0,61 \pm 0,08$ Unpaired t test $t=0.8576$ $p>0.05$ **Fig. 4L**). These data indicate
495 that the decrease in AMPA/NMDA ratio specifically observed at motor cortex to DLS
496 synapses was not accompanied by major changes in AMPAR-mediated transmission and
497 suggest therefore that the reduction of the ratio may be the consequence of an increase in
498 NMDA-mediated current.

499

500 To better describe possible changes in NMDAR-mediated current at motor cortex to DLS
501 synapses, we pharmacologically isolated optogenetically-induced NMDAR currents and
502 characterized the NMDAR subunit composition. NMDA-EPSC recorded from YAC128 mice
503 presented a slower decay time (WT $110 \pm 4,1$ ms, n=16 neurons; YAC128 $152,5 \pm 17,72$ ms
504 n=12 neurons Unpaired t -test $t(26)=2.662$ $p<0.05$ **Fig. 4H**) and an increased ifenprodil
505 sensitivity (WT $57,76 \pm 3.42$ % n= 7 neurons ; YAC128 73.67 ± 5.01 % n=7 neurons
506 Unpaired t-test $t(12)=2.621$ $p<0.05$ **Fig. 4I-J**). Furthermore, we could not find changes in
507 current/voltage relationship compared to control mice (WT n= 7 neurons, YAC128 n= 7
508 neurons **Fig. 4K**). These data indicated an enriched GluN2B subunit composition at motor
509 cortex to DLS synapses at early stages of HD diseases but no changes in GluN3A contents.

510

511 NMDAR subunit composition is crucial for the induction of Long Term Depression (LTD) in
512 the DLS (Brigman et al., 2010). We predicted that changes in NMDAR current would
513 therefore impact the induction of this form of synaptic plasticity. We observed that 1Hz
514 stimulation for 5 min induced a significantly stronger NMDA-dependent Long-Term
515 Depression (LTD) at motor cortex to DLS synapses in YAC128 compared to control mice
516 (Two way ANOVA interaction effect $F(1,35)=10.45$ $p= 0.0027$ followed by a Bonferroni
517 post hoc WT : 28.21 ± 5.84 % of depression, n=12 neurons vs YAC128 69.31 ± 2.81 % of
518 depression n= 13 neurons , $p<0.0001$ **Fig. 5A, B, D**). However, when we blocked the NMDA
519 receptor with APV, we did not observe changes between genotypes in the magnitude of the
520 LTD (YAC128 69.31 ± 2.81 % of depression vs YAC128 + APV 20.54 ± 2.48 % (n= 6
521 neurons) of depression $p<0.0001$ **Fig. 5C, D**). In addition, this stimulation protocol didn't

522 elicit changes in paired pulse ratio in both groups (WT pre: 0.82 ± 0.02 ; WT post: $0.74 \pm$
523 0.05 , $n= 7$ neurons paired t-test $t=1.593$ $p>0.05$; YAC128 pre: 0.52 ± 0.12 ; YAC128 post
524 $:0.42 \pm 0.13$, $n= 4$ neurons paired t-test $t=0.5259$ $p>0.05$ **Fig. 5E, F**).

525 Altogether these data indicate that at early stage of HD disease there are specific changes in
526 NMDA-mediated currents at motor cortex to DLS synapses and that these changes prime the
527 synapses for changes in NMDA-dependent form of synaptic plasticity.

528

529 Finally, we tested whether input specific changes in NMDAR-mediated transmission relate to
530 deficits in motor skills consolidation. We injected mice with ChR2 expressing virus in the
531 motor cortex in control and YAC128 mice and 6 weeks after the injection we performed
532 single pellet reaching task (**Fig 6A**). Five minutes after the last training session (day 8 and 9,
533 WT= 3.135 ± 0.495 , $N=2$ mice, YAC128 = 0.675 ± 0.67 , $N=2$ mice, **Fig 6B**), we sacrificed
534 the animals and cut coronal slices. Interestingly we found that motor training promoted a
535 decrease in AMPA/NMDA ratio at motor cortex to DLS synapses in WT mice (WT naïve:
536 0.632 $n= 6$ neurons, WT after Single pellet: 0.279 $n= 12$ neurons; YAC128 naïve: 0.424 $n= 7$
537 neurons, YAC128 after single pellet: 0.358 , $n= 8$ neurons, Two way Anova interaction effect
538 $F(1,31)=9.282$, $p<0.05$ followed by Bonferroni post hoc WT naïve vs YAC128 naïve
539 $p<0.05$; WT naïve vs WT after single pellet $p<0.001$, **Fig. 6B-C**). Remarkably we found that
540 motor skills learning-induced synaptic plasticity was absent in YAC128 mice (**Fig. 6B**).

541 These data not only indicated a circuit-specific form of synaptic plasticity associated with
542 motor skills consolidation but also suggest that this form of plasticity is needed during the
543 consolidation of motor skill learning.

544

545

546

547

548

549

550

551 **DISCUSSION**

552 We found that 3-month-old YAC128 mice present deficits in consolidation phase of
553 motor skill learning compared to WT without major motor dysfunctions. While during initial
554 task exposition, motor abilities were equivalent between groups, control mice maintained
555 their newly acquired motor skill across training both in rotarod and single pellet reaching

556 tasks whereas YAC128 mice did not. Associated to these alterations, we showed a specific
557 decrease in AMPA/NMDA ratio at motor cortex to DLS synapses in YAC128 mice. Together
558 with a modified NMDAR transmission and enhanced ifenprodil sensitivity in motor cortex to
559 DLS synapses in these mice, we also observed an aberrant NMDAR-dependent LTD induced
560 by optogenetic low frequency stimulation protocol. Moreover, we highlighted that synaptic
561 plasticity induced by single pellet reaching task training at motor cortex to DLS synapses was
562 occluded in YAC128 mice.

563

564 As previously reported (Chiu et al., 2011) and contrary to another report (Slow et al.,
565 2003) we did not observe changes in locomotor activity in YAC128 mice compared to
566 control between 11 and 14 weeks in the circular corridor and in the open field task. Despite
567 the absence of any gross motor impairment, here for the first time we observed a deficit in
568 motor skill consolidation in YAC128 compared to wild type. Intriguingly YAC128 and
569 control mice presented an equivalent motor performance during early phases of motor
570 learning. Remarkably, while WT mice maintained their acquired learning, YAC128 mice
571 showed a worsening of the motor skills after a break in the training session suggesting that
572 YAC128 mice present deficits in the consolidation of motor skill learning. Despite YAC128
573 mice from C57B6/J background strain which express the htt mutant transgene are not the
574 strain that present the strongest phenotype severity compared to YAC128 mice from a
575 FVB/N background strain (Van Raamsdonk et al 2007), here we have shown that motor
576 consolidation deficits are detected at early stage in this mouse model of Huntington's disease.
577 One limitation of this present study is the potential difference in parental behavior that we
578 can't exclude with our breeding strategy between wild-type C57B6/J control mice and
579 YAC128 homozygous from C57 B6/J background (see details in the material and methods
580 section). Future studies will be needed to investigate whether these deficits are specific
581 within the context of motor learning or if more general deficits in memory consolidation
582 could be observed in these mice.

583 In this study, we highlighted the importance to distinguish prior initial motor
584 performance from motor skill acquisition and consolidation in order to better detect
585 phenotype abnormality in YAC128 mice. Previous studies have already pinpointed motor
586 dysfunctions in YAC128 mice in the rotarod without defining whether the defects were due
587 to a motor learning impairment or rather a deficit in the consolidation of prior newly acquired
588 motor skill (Pouladi et al 2009, Van Raamsdonk et al 2007). Learning new skills is
589 characterized by an initial phase of rapid improvement followed by a more gradual phase of

590 progress as skills are automatized. Interestingly, region-specific changes in neuronal activity
591 and synaptic plasticity in the striatum have been observed during acquisition and
592 consolidation of motor skills (Yin et al 2009). Using the single pellet reaching task to observe
593 the acquisition and consolidation of new motor skills (Karni et al 1998), our data support the
594 findings that motor cortex to DLS plasticity during extended training is necessary to the
595 consolidation of motor skills. Importantly, skill reaching task can be considered as a useful
596 motor learning task that can be performed in premanifest HD mouse model where new
597 alternative protective treatments may be tested with a strong potential translational
598 perspective for HD patients (Klein et al., 2011; 2012). Consequently, a detailed analysis of
599 distinct motor tasks seems essential to better dissect motor alterations in initial stage of the
600 disease both in rodents and in humans.

601

602 Although we decreased potent stressful environmental effects and considered anxiogenic
603 traits of YAC128 mice by performing handling, habituation and using low light setting
604 conditions, motor tasks cannot be exclusively restricted to motor function. Indeed, deficits in
605 motor task performance could be the consequence of anxiety phenotype, attention and/or
606 motivation deficits. The increase floating behavior during the swimming tank test and
607 decrease time in open arms in the elevated plus maze suggest that premanifest HD mice
608 present anxiety-like and depressive-like phenotypes. Interestingly, previous studies have
609 reported similar results in YAC128 mice and in the R6/2 mice model of Huntington disease
610 (Carter et al., 1999; Chiu et al., 2011). Future studies will need to further investigate these
611 behavioural traits in YAC128 mice and examine the relevant circuits. Importantly, we
612 reported the same number of total attempts in single pellet reaching task across days in WT
613 and YAC128 mice suggesting that both groups attempt to perform this task. Concerning
614 anhedonia evaluation of YAC128 mice, we found different results with sucrose consumption
615 experiment compared to Pouladi et al. 2009. These apparent discrepancies may be first
616 explained by distinct protocols. First, in Pouladi et al. study, mice were only exposed one
617 time to the 2 % sucrose solution which design cannot exclude the potential confounding
618 effect induced by neophobia without previous food restriction. In our present study, we
619 wanted to evaluate the sucrose preference of mice that underwent a single reaching motor
620 learning under food restriction condition. We therefore exposed during 2 days the animals to
621 1 % of sucrose solution to avoid any confounding effect of the first exposure of sucrose
622 followed by 8% sucrose solution exposure. Under these specific conditions, we didn't detect
623 difference in the sucrose consumption. In addition, we used different mice background (in

624 our study: YAC128 from C57 B6/J vs YAC128 from FVB/N background in Pouladi et al
625 2009). As reported in Van Raamsdonk et al 2007, YAC transgene expressing mutant htt is
626 penetrant on both background but the severity is modulated by strain which may also explain
627 these differences. Even if no major anhedonia has been suggested here, the integrity of
628 reward circuits and of dopamine neuromodulation should be further investigated notably by
629 assessing a progressive ratio schedule to control for any general impairment in general
630 motivation in YAC128 mice.

631

632 Previous studies pinpointed abnormalities in glutamatergic transmission onto MSN in
633 different HD mouse model across ages (André et al., 2011; Marco et al., 2013). Despite of no
634 significant changes in the PPR at motor cortex to dorsolateral striatum, we noted a trend at
635 100 ms pulse interval (**Fig. 4L**) in YAC128 mice suggesting that further changes in
636 presynaptic release properties may appear at later stages of the disease. It has been shown
637 that striatal MSNs express higher level of extrasynaptic NMDARs at pre-symptomatic stages
638 (Okamoto et al., 2009; Milnerwood et al., 2010) and that changes in NMDAR localization are
639 independent of the source of glutamatergic input (Kolodziejczyk and Raymond, 2016). Here,
640 we unraveled specific deficiencies of glutamatergic transmission at motor cortex to DLS
641 synapses whereas no AMPA/NMDA ratio changes were observed at thalamo-striatal
642 synapses or at motor cortex to DMS synapses (data not shown) at that stage neither. In the
643 present study, we used both males and females. Despite we didn't perform statistical analysis
644 for a specific sex effect, we found important to display males and females data. It will be
645 interesting to further extend this study on sex differences with the progression of HD.

646

647 Motor learning deficit in HD mouse models have been linked to deficits in striatal plasticity
648 and to aberrant function of NMDARs. Indeed, deletion of striatal NMDAR abolished striatal
649 LTP and impaired learning (Dang et al., 2006). Furthermore, R6/2 mice show less NMDA-
650 dependent LTP in the striatum compared to WT control (Kung et al., 2007) while deficit in
651 endocannabinoid-dependent LTD was observed in the YAC128 mice (Sepers et al., 2018).
652 Here we show that at motor cortex to DLS synapses, the increased contribution of NMDAR
653 is accompanied by an increase in GluN2B-containing NMDARs. Interestingly, an increase in
654 NMDAR-mediated over an AMPAR-mediated current has been shown in DLS synapses after
655 extended motor training (Yin et al., 2009). Here we show that synaptic plasticity induced by
656 motor learning does not occur in YAC128 mice suggesting that the increased number of
657 NMDARs at motor cortex occludes the motor learning dependent insertion of NMDARs.

658 Remarkably we also found that NMDA-dependent LTD is aberrant at motor cortex to DLS
659 synapses suggesting that depotentiation of NMDA synaptic transmission in this pathway may
660 restore synaptic transmission and may therefore represent a possible therapeutic intervention.

661

662 In general, this study proposed new meaningful insight in the synaptopathic mechanisms of
663 HD. We highlight that deficit in motor skill consolidation-dependent synaptic plasticity at
664 motor cortex to DLS synapses represents an early biomarker for Huntington's disease. Lastly,
665 we encourage detailed motor investigations at premanifest stage to further screen new
666 potential therapeutically preventive strategies for HD.

667

668

669

670 **References**

671 André VM, Cepeda C, Fisher YE, Huynh M, Bardakjian N, Singh S, Yang XW, Levine MS
672 (2011) Differential electrophysiological changes in striatal output neurons in
673 Huntington's disease. *J Neurosci* 31:1170–1182.

674 Brigman JL, Wright T, Talani G, Prasad-Mulcare S, Jinde S, Seabold GK, Mathur P, Davis
675 MI, Bock R, Gustin RM, Colbran RJ, Alvarez VA, Nakazawa K, Delpire E, Lovinger
676 DM, Holmes A (2010) Loss of GluN2B-containing NMDA receptors in CA1
677 hippocampus and cortex impairs long-term depression, reduces dendritic spine density,
678 and disrupts learning. *J Neurosci* 30:4590–4600.

679 Carter RJ, Lione LA, Humby T, Mangiarini L, Mahal A, Bates GP, Dunnett SB, Morton AJ
680 (1999) Characterization of progressive motor deficits in mice transgenic for the human
681 Huntington's disease mutation. *J Neurosci* 19:3248–3257.

682 Chen, C. C., Gilmore, A., Zuo, Y. (2014) Study Motor Skill Learning by Single-pellet
683 Reaching Tasks in Mice. *J. Vis. Exp.* (85), e51238.

684 Chiu C-T, Liu G, Leeds P, Chuang D-M (2011) Combined treatment with the mood
685 stabilizers lithium and valproate produces multiple beneficial effects in transgenic mouse
686 models of Huntington's disease. *Neuropsychopharmacology* 36:2406–2421.

687 Choi, S., & Lovinger, D. M. (1997). Decreased Frequency But Not Amplitude of Quantal
688 Synaptic Responses Associated with Expression of Corticostriatal Long-Term
689 Depression. *The Journal of Neuroscience*, 17(21), 8613–8620.

690 Dang MT, Yokoi F, Yin HH, Lovinger DM, Wang Y, Li Y (2006) Disrupted motor learning
691 and long-term synaptic plasticity in mice lacking NMDAR1 in the striatum. *Proc Natl*
692 *Acad Sci USA* 103:15254–15259.

- 693 de Boo GM, Tibben A, Lanser JB, Jennekens-Schinkel A, Hermans J, Maat-Kievit A, Roos
694 RA (1997) Early cognitive and motor symptoms in identified carriers of the gene for
695 Huntington disease. *Arch Neurol* 54:1353–1357.
- 696 Duff K, Beglinger LJ, Paulsen JS (2008) “Pre-symptomatic” Huntington's disease. *Handb*
697 *Clin Neurol* 89:589–598.
- 698 Giralt A, Saavedra A, Alberch J, Pérez-Navarro E (2012) Cognitive Dysfunction in
699 Huntington's Disease: Humans, Mouse Models and Molecular Mechanisms. *J*
700 *Huntingtons Dis* 1:155–173.
- 701 Guo Q, Wang D, He X, Feng Q, Lin R, Xu F, Fu L, Luo M (2015) Whole-brain mapping of
702 inputs to projection neurons and cholinergic interneurons in the dorsal striatum. *Arenkiel*
703 *B, ed. PLoS ONE* 10:e0123381.
- 704 Karni, A., Meyer, G., Rey-Hipolito, C., Jezzard, P., Adams, M. M., Turner, R., &
705 Ungerleider, L. G. (1998). The acquisition of skilled motor performance: Fast and slow
706 experience-driven changes in primary motor cortex. *Proceedings of the National*
707 *Academy of Sciences*, 95(3).
- 708 Kirkwood SC, Siemers E, Hodes ME, Conneally PM, Christian JC, Foroud T (2000) Subtle
709 changes among presymptomatic carriers of the Huntington's disease gene. *J Neurol*
710 *Neurosurg Psychiatry* 69:773–779.
- 711 Kirkwood SC, Siemers E, Stout JC, Hodes ME, Conneally PM, Christian JC, Foroud T
712 (1999) Longitudinal cognitive and motor changes among presymptomatic Huntington
713 disease gene carriers. *Arch Neurol* 56:563–568.
- 714 Klein A, Sacrey L-AR, Dunnett SB, Whishaw IQ, Nikkhah G (2011) Proximal movements
715 compensate for distal forelimb movement impairments in a reach-to-eat task in
716 Huntington's disease: new insights into motor impairments in a real-world skill.
717 *Neurobiol Dis* 41:560–569.
- 718 Klein A, Sacrey L-AR, Whishaw IQ, Dunnett SB (2012) The use of rodent skilled reaching
719 as a translational model for investigating brain damage and disease. *Neurosci Biobehav*
720 *Rev* 36:1030–1042.
- 721 Kolodziejczyk K, Raymond LA (2016) Differential changes in thalamic and cortical
722 excitatory synapses onto striatal spiny projection neurons in a Huntington disease mouse
723 model. *Neurobiol Dis* 86:62–74.
- 724 la Monte de SM, Vonsattel JP, Richardson EP (1988) Morphometric demonstration of
725 atrophic changes in the cerebral cortex, white matter, and neostriatum in Huntington's
726 disease. *J Neuropathol Exp Neurol* 47:516–525.
- 727 Lambot L, Chaves Rodriguez E, Houtteman D, Li Y, Schiffmann SN, Gall D, de Kerchove
728 d'Exaerde A (2016) Striatopallidal Neuron NMDA Receptors Control Synaptic
729 Connectivity, Locomotor, and Goal-Directed Behaviors. *J Neurosci* 36:4976–4992.
- 730 Levine MS, Klapstein GJ, Koppel A, Gruen E, Cepeda C, Vargas ME, Jokel ES, Carpenter
731 EM, Zanjani H, Hurst RS, Efstratiadis A, Zeitlin S, Chesselet MF (1999) Enhanced

- 732 sensitivity to N-methyl-D-aspartate receptor activation in transgenic and knockin mouse
733 models of Huntington's disease. *J Neurosci Res* 58:515–532.
- 734 Mahfooz K, Marco S, Martínez-Turrillas R, Raja MK, Perez-Otano I, Wesseling JF (2016)
735 GluN3A promotes NMDA spiking by enhancing synaptic transmission in Huntington's
736 disease models. *Neurobiol Dis* 93:47–56.
- 737 Marco S, Giralt A, Petrovic MM, Pouladi MA, Martínez-Turrillas R, Martínez-Hernández J,
738 Kaltenbach LS, Torres-Peraza J, Graham RK, Watanabe M, Luján R, Nakanishi N,
739 Lipton SA, Lo DC, Hayden MR, Alberch J, Wesseling JF, Perez-Otano I (2013)
740 Suppressing aberrant GluN3A expression rescues synaptic and behavioral impairments in
741 Huntington's disease models. *Nat Med* 19:1030–1038.
- 742 Marco, S., Murillo, A., & Pérez-Otaño, I. (2018). RNAi-Based GluN3A Silencing Prevents
743 and Reverses Disease Phenotypes Induced by Mutant huntingtin. *Molecular Therapy*,
744 26(8), 1965–1972.
- 745 Milnerwood AJ, Gladding CM, Pouladi MA, Kaufman AM, Hines RM, Boyd JD, Ko RWY,
746 Vasuta OC, Graham RK, Hayden MR, Murphy TH, Raymond LA (2010) Early increase
747 in extrasynaptic NMDA receptor signaling and expression contributes to phenotype onset
748 in Huntington's disease mice. *Neuron* 65:178–190.
- 749 Milnerwood AJ, Raymond LA (2010) Early synaptic pathophysiology in neurodegeneration:
750 insights from Huntington's disease. *Trends Neurosci* 33:513–523.
- 751 Okamoto S-I, Pouladi MA, Talantova M, Yao D, Xia P, Ehrnhoefer DE, Zaidi R, Clemente
752 A, Kaul M, Graham RK, Zhang D, Vincent Chen H-S, Tong G, Hayden MR, Lipton SA
753 (2009) Balance between synaptic versus extrasynaptic NMDA receptor activity
754 influences inclusions and neurotoxicity of mutant huntingtin. *Nat Med* 15:1407–1413.
- 755 Paoletti P, Bellone C, Zhou Q (2013) NMDA receptor subunit diversity: impact on receptor
756 properties, synaptic plasticity and disease. *Nature Publishing Group* 14:383–400.
- 757 Pouladi MA, Graham RK, Karasinska JM, Xie Y, Santos RD, Petersén A, Hayden MR
758 (2009) Prevention of depressive behaviour in the YAC128 mouse model of Huntington
759 disease by mutation at residue 586 of huntingtin. *Brain* 132:919–932.
- 760 Schneider SA, Wilkinson L, Bhatia KP, Henley SMD, Rothwell JC, Tabrizi SJ, Jahanshahi M
761 (2010) Abnormal explicit but normal implicit sequence learning in premanifest and early
762 Huntington's disease. *Mov Disord* 25:1343–1349.
- 763 Sepers MD, Smith-Dijak A, LeDue J, Kolodziejczyk K, Mackie K, Raymond LA (2018)
764 Endocannabinoid-Specific Impairment in Synaptic Plasticity in Striatum of Huntington's
765 Disease Mouse Model. *J Neurosci* 38:544–554.
- 766 Shabbott B, Ravindran R, Schumacher JW, Wasserman PB, Marder KS, Mazzoni P (2013)
767 Learning fast accurate movements requires intact frontostriatal circuits. *Front Hum*
768 *Neurosci* 7:752.
- 769 Slow EJ, van Raamsdonk J, Rogers D, Coleman SH, Graham RK, Deng Y, Oh R, Bissada N,
770 Hossain SM, Yang Y-Z, Li X-J, Simpson EM, Gutekunst C-A, Leavitt BR, Hayden MR

- 771 (2003) Selective striatal neuronal loss in a YAC128 mouse model of Huntington disease.
772 *Hum Mol Genet* 12:1555–1567.
- 773 Smith Y, Raju DV, Pare J-F, Sidibe M (2004) The thalamostriatal system: a highly specific
774 network of the basal ganglia circuitry. *Trends Neurosci* 27:520–527.
- 775 Southwell AL, Ko J, Patterson PH (2009) Intrabody gene therapy ameliorates motor,
776 cognitive, and neuropathological symptoms in multiple mouse models of Huntington's
777 disease. *J Neurosci* 29:13589–13602.
- 778 Tabrizi SJ, Langbehn DR, Leavitt BR, Roos RA, Durr A, Craufurd D, Kennard C, Hicks SL,
779 Fox NC, Scahill RI, Borowsky B, Tobin AJ, Rosas HD, Johnson H, Reilmann R,
780 Landwehrmeyer B, Stout JC, TRACK-HD Investigators (2009) Biological and clinical
781 manifestations of Huntington's disease in the longitudinal TRACK-HD study: cross-
782 sectional analysis of baseline data. *Lancet Neurol* 8:791–801.
- 783 Tabrizi SJ, Scahill RI, Durr A, Roos RA, Leavitt BR, Jones R, Landwehrmeyer GB, Fox NC,
784 Johnson H, Hicks SL, Kennard C, Craufurd D, Frost C, Langbehn DR, Reilmann R,
785 Stout JC, TRACK-HD Investigators (2011) Biological and clinical changes in
786 premanifest and early stage Huntington's disease in the TRACK-HD study: the 12-month
787 longitudinal analysis. *Lancet Neurol* 10:31–42.
- 788 Van Raamsdonk JM, Metzler M, Slow E, Pearson J, Schwab C, Carroll J, Graham RK,
789 Leavitt BR, Hayden MR (2007) Phenotypic abnormalities in the YAC128 mouse model
790 of Huntington disease are penetrant on multiple genetic backgrounds and modulated by
791 strain. *Neurobiol Dis* 26:189–200.
- 792 Van Raamsdonk JM, Pearson J, Slow EJ, Hossain SM, Leavitt BR, Hayden MR (2005)
793 Cognitive dysfunction precedes neuropathology and motor abnormalities in the YAC128
794 mouse model of Huntington's disease. *J Neurosci* 25:4169–4180.
- 795 Wall NR, La Parra De M, Callaway EM, Kreitzer AC (2013) Differential innervation of
796 direct- and indirect-pathway striatal projection neurons. *Neuron* 79:347–360.
- 797 Wolf RC, Grön G, Sambataro F, Vasic N, Wolf ND, Thomann PA, Saft C, Landwehrmeyer
798 GB, Orth M (2012) Brain activation and functional connectivity in premanifest
799 Huntington's disease during states of intrinsic and phasic alertness. *Hum Brain Mapp*
800 33:2161–2173.
- 801 Yin HH, Mulcare SP, Hilário MRF, Clouse E, Holloway T, Davis MI, Hansson AC, Lovinger
802 DM, Costa RM (2009) Dynamic reorganization of striatal circuits during the acquisition
803 and consolidation of a skill. *Nature Neuroscience* 12:333–341.
- 804
- 805
- 806
- 807
- 808
- 809

818 **FIGURE LEGENDS**819 **Fig. 1. Motor consolidation alterations in swimming tank test and rotarod task in**
820 **premanifest stage in YAC128 mice.**

821 **A, D.** activity trail plots. **B, E.** Group mean of the distance travelled in circular corridor (b) or
822 in open field (e) in WT and YAC128 mice. **C, F.** Group mean of the velocity in circular
823 corridor (c) or in open field (f) in WT and YAC128 mice. **G.** experimental schematic. **H.**
824 Time course of cross latency in swimming tank test in WT and YAC128 mice. **I.**
825 Quantification of failed trials at day 2 and day 7 of swimming tank test in WT and YAC128
826 mice. **J.** Quantification of floating behaviour across training in YAC128 mice. **K.** Floating
827 behaviour across swimming tank test training in YAC128 mice. Each horizontal line
828 represents the floating behaviour of an individual mouse during the 30 s trial for the trial 1
829 (t1), the trial 2 (t2) and the trial 3 (t3) at day1, day 2, day 3 and day7. Each episode of
830 floating behaviour is represented in dark blue. Females are represented in blue color while
831 male mice are labelled in red color. **L.** Experimental schematic. **M.** Group mean of the time
832 in open arms expressed in percentage in the elevated plus maze WT and YAC128 mice. **N.**
833 Experimental schematic. **O.** Time course of the fall latency in rotarod in WT and YAC128
834 mice. Square symbols represent female mice and circles represent males. Error bars show
835 SEM. *M.:* male, *F.:* female. * $p < 0.05$, ** $p < 0.01$, *** $p < 0.001$. ### $p < 0.001$ YAC D7 vs
836 WT D7.

837

838

839 **Fig. 2. Forelimb motor skill consolidation is impaired in premanifest stage in YAC128**
840 **mice.**

841 **A, B.** Timeline (a) and experimental schematic (b) of single pellet reaching task. **C.** Heat map
842 of successful attempts in WT and YAC128 mice at day 1 and day 8. Each horizontal line in
843 the heat map represents the performance of an individual mouse. Each vertical white line
844 represents the time to reach 50 % of the pellets. **D.** Average speed of success over the training
845 phase of single pellet reaching task in WT and YAC128 mice. **E, F.** Scatter plot and group
846 mean of the success rate at day 1 versus day 8 of the single pellet reaching task within WT (e)
847 and YAC128 mice (f). **G.** Kinetic of total attempts (including success, drop and failed
848 attempts) across single pellet reaching task training days in WT and YAC128 mice. **H.**
849 Kinetic of fail rate and drop rate during single pellet training in WT and YAC128 mice. **I.**
850 Experimental schematic. **J.** Group mean sucrose consumption across days. **K.** Group mean
851 water consumption across days. **L.** Group mean sucrose consumption normalized to

852 bodyweight across days. **M.** Sucrose preference at day 1, day 2 and day 3 in WT and
 853 YAC128 mice. Square symbols represent female mice and circles represent males. Error bars
 854 show SEM. *** $p < 0.001$.

855

856 **Fig. 3. No major differences on synaptic strength with electrical stimulation in YAC128**
 857 **MSN.**

858 **A.** Experimental schematic. **B.** Group mean Paired Pulse Ratio for WT and YAC128 MSN.
 859 Right: example traces of AMPAR-EPSC at -60 mV in WT and YAC128 MSN. Scale bar 20
 860 ms, 50 pA. **C.** Group mean amplitude and frequency of asynchronous evoked events in WT
 861 and YAC128 MSN. Right: example traces of evoked AMPAR-aEPSCs recorded at -70 mV.
 862 Star indicating an asynchronous event detected. Scale bar 50 ms, 25 pA. **D.** Group mean
 863 AMPA/NMDAR ratio calculated in WT and YAC128 MSN. Right: example traces of evoked
 864 AMPAR- and NMDAR-EPSCs at + 40 mV. Scale bar 20 ms, 50 pA. **E.** Group mean RI
 865 calculated in WT and YAC128 MSN. Right: example traces of evoked AMPAR-EPSCs
 866 recorded at -60 mV, 0 mV and + 40 mV. Scale bar 20 ms, 50 pA. **F.** Time course of
 867 NMDAR-EPSC amplitude during ifenprodil application for WT and YAC128 MSN and
 868 associated example traces in WT and YAC128 mice in the inset. **G.** Group mean ifenprodil
 869 inhibition calculated in WT and YAC128 MSN. Scale bar 50 ms, 50 pA. Square symbols
 870 represent female mice and circles represent males.

871

872 **Fig. 4. NMDAR transmission dysfunction at motor cortex to DLS MSN in YAC128 mice.**

873 **A.** Left: Experimental schematic; left down: *in vitro* validation of 20 Hz blue light
 874 stimulation protocol. Scale: 0.1s, 10 mV; right: epifluorescent image of AAV5-CamKII-
 875 hChR2(H134R)-EGFP injection in the thalamus (top) or in the Motor Cortex (down). **B, C.**
 876 Group mean AMPA/NMDAR ratio calculated in WT and YAC128 MSN at thalamo-
 877 dorsolateral synapses (b) or at motor cortex to dorsolateral synapses (c). Right: example
 878 traces of evoked AMPAR- and NMDAR-EPSCs at + 40 mV. scale bar b) 50 ms, 25 pA and
 879 c) 10 ms, 50 pA. **D.** Group mean AMPA/NMDAR ratio calculated in WT-D1⁺ MSN, WT-D1⁻
 880 MSN, YAC128-D1⁺ MSN and YAC128-D1⁻ MSN at motor cortex to dorsolateral synapses.
 881 Scale bar 10 ms, 50 pA. **E.** Group mean RI calculated at motor cortex to DLS synapses in
 882 WT and YAC128 MSN. Right: example traces of evoked AMPAR-EPSCs recorded at -60
 883 mV, 0 mV and + 40 mV. Scale bar 10 ms, 50 pA for YAC128 and scale bar 10 ms, 50 pA for
 884 WT. **F.** I-O relationship of motor cortex glutamatergic transmission established by the

885 stimulation duration (synaptic input) and the amplitude of the EPSC (output) in slices from
886 WT and YAC128 MSN. Right: Representative EPSCs evoked by motor cortex terminal
887 stimulation in dorsolateral striatum recorded at -60 mV in WT and YAC128 MSN. Scale bar
888 10 ms, 50 pA. **G.** Group mean amplitude of asynchronous evoked events in WT and YAC128
889 MSN. Right: example traces of evoked AMPAR-aEPSCs recorded at - 70 mV. Star
890 indicating an asynchronous event detected Scale bar 50 ms, 25 pA. **H.** Group mean decay
891 time of NMDAR-EPSCs at + 40 mV in WT and YAC128 MSN. Right: example traces of
892 NMDAR-EPSC at + 40 mV. **I.** Time course of NMDAR-EPSC amplitude during ifenprodil
893 application for WT and YAC128 MSN. Scale bar 15 ms. **J.** Group mean ifenprodil inhibition
894 calculated in WT and YAC128 MSN. Right: example traces of NMDAR-EPSCs during
895 ifenprodil (3 μ M) bath application. Scale bar 20 ms, 25 pA. **K.** I-V plots of normalized and
896 averaged NMDAR-EPSCs of motor cortex to dorsolateral striatal MSN in WT and YAC128
897 mice and their associated example traces. Scale bar 50 ms, 50 pA. **L.** Group mean Paired
898 Pulse Ratio recorded at interval of 50, 100, 300 ms for WT and YAC128 MSN evoked by
899 motor cortex stimulation. Right: example traces of AMPAR-EPSC at -60 mV in WT and
900 YAC128 MSN. Scale bar 50 ms, 25 pA. Square symbols represent female mice and circles
901 represent males.

902

903

904 **Fig. 5. Aberrant NMDAR dependent LTD at motor cortex to DLS MSN in YAC128**
905 **mice**

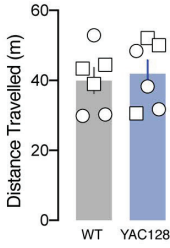
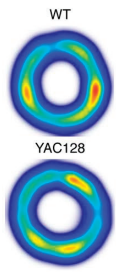
906 **A.** Experimental schematic. **B, C.** Kinetic of AMPA EPSC amplitude normalized to baseline
907 at motor cortex to DLS MSN after low frequency stimulation (1Hz, 5min) in WT and
908 YAC128 groups with picrotoxin (50 μ M) (b) or with picrotoxin and APV (30 μ M) (c). *Top:*
909 example traces pre and post 1 Hz, 5min. **D.** Quantification of AMPA EPSC amplitude
910 normalized to baseline at motor cortex to DLS MSN after low frequency stimulation in WT
911 and YAC128 groups without and with APV application. **E, F.** Paired pulse ratio pre and post
912 low frequency stimulation protocol at motor cortex to DLS MSN in WT (e) and YAC128
913 mice (f). Scales bar 20 ms, 50 pA. Square symbols represent female mice and circles
914 represent males. Error bars show SEM. **** $p < 0.0001$

915

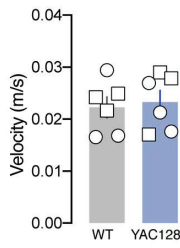
916 **Figure 6. Motor training induced motor cortex to DLS MSN plasticity is occluded in**
917 **YAC128 mice.**

918 A. Experimental schematic. B. Average speed of success at the end of the training phase of
919 single pellet reaching task (day 8- day 9) in WT and YAC128 mice. C, D. Group mean
920 AMPA/NMDAR ratio calculated in WT and YAC128 MSN in naïve group or after single
921 pellet reaching task training. Right: example traces of evoked AMPAR- and NMDAR-EPSCs
922 at + 40 mV. Scales bar 50 ms, 100 pA. Error bars show SEM.
923

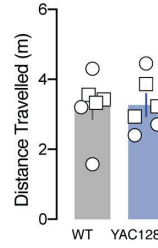
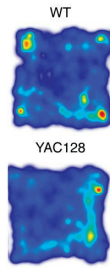
A Circular corridor



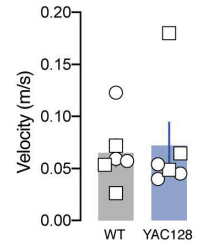
C



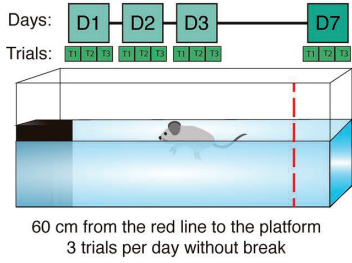
D Open field



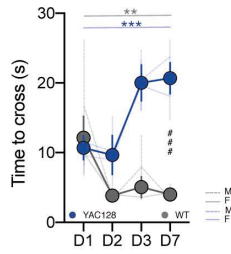
F



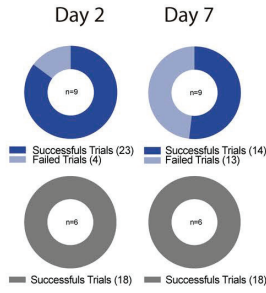
G Swimming tank test



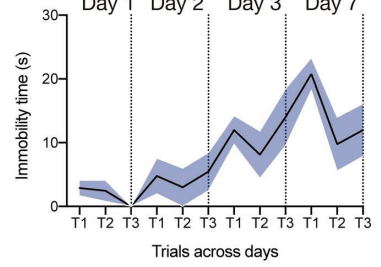
H All trials



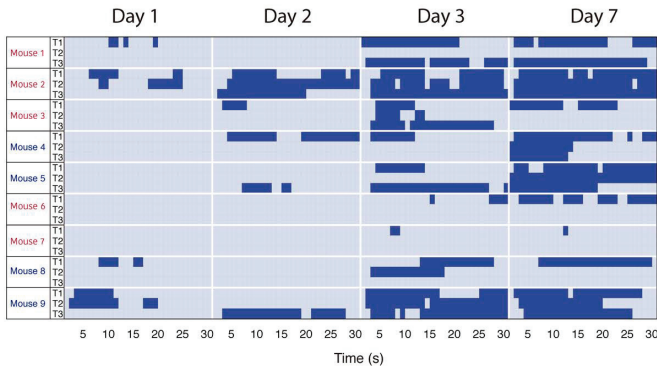
I Failed trials



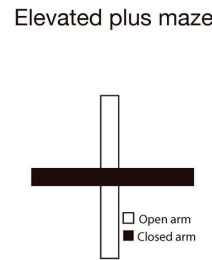
J Floating behavior



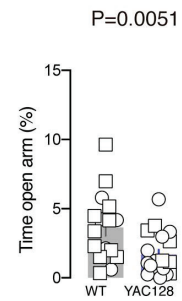
K Floating behavior across days YAC 128



L



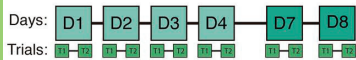
M



N

Rotarod training

5 RPM to 40 RPM within 240s
2 trials per day with 10 min break



O

Training

